

The proton radius puzzle

Maurizio Bonesini^{1,a}

¹ *Sezione INFN Milano Bicocca, Dipartimento di Fisica G. Occhialini, Milano, Italy*
(on behalf of the **FAMU Collaboration**)

Abstract. The FAMU (Fisica degli Atomi Muonici) experiment has the goal to measure precisely the proton Zemach radius, thus contributing to the solution of the so-called proton radius “puzzle”. To this aim, it makes use of a high-intensity pulsed muon beam at RIKEN-RAL impinging on a cryogenic hydrogen target with an high-Z gas admixture and a tunable mid-IR high power laser, to measure the hyperfine (HFS) splitting of the 1S state of the muonic hydrogen. From the value of the exciting laser frequency, the energy of the HFS transition may be derived with high precision ($\sim 10^{-5}$) and thus, via QED calculations, the Zemach radius of the proton. The experimental apparatus includes a precise fiber-SiPMT beam hodoscope and a crown of eight $LaBr_3$ crystals and a few HPGe detectors for detection of the emitted characteristic X-rays. Preliminary runs to optimize the gas target filling and its operating conditions have been taken in 2014 and 2015-2016. The final run, with the pump laser to drive the HFS transition, is expected in 2018.

1 Introduction: the proton radius puzzle

Many properties of the proton - the primary visible universe building block- such as its radius and anomalous magnetic moment, are not completely understood. The so-called proton radius “puzzle” [1] refers to the 7σ discrepancy between the electron and muon determination of the proton charge radius. This discrepancy may be due to a violation of the electron-muon universality or simply to not well understood experimental problems.

The precise measurement of the Zemach radius of the proton with muons may shed new light on the problem. Table 1 resumes the current experimental situation for both the proton charge (r_{ch}) and Zemach radius (r_Z) determination with muons or electrons.

2 The FAMU experimental method

The experimental method to be used by the FAMU Collaboration [7] is shown schematically in figure 1. It makes use of a high intensity pulsed low-energy muon beam, stopping in a hydrogen target, to produce muonic hydrogen (in a mixture of singlet $F=0$ and triplet $F=1$ states) and a tunable mid-IR high power laser to excite the hyperfine splitting (HFS) transition of the 1S muonic hydrogen (from $F=0$ to $F=1$ states). Exploiting the muon transfer from muonic hydrogen to another higher-Z gas in the target (such as O_2 or Ar), the $\mu^- p_{1S}$ HFS transition will be recognized by an increase of the number of X-rays from the (μZ^*) cascade, while tuning the laser frequency ν_0 ($\Delta E_{HFS} = h\nu_0^{res}$).

^ae-mail: maurizio.bonesini@mib.infn.it

Table 1. The present situation of the proton charge and Zemach radius measurements.

	charge radius $r_{ch}(\text{fm})$	Zemach radius $r_Z(\text{fm})$
e-p scattering and hydrogen spectroscopy	$\langle r_{ch} \rangle = 0.8751(61)$ [6]	$r_Z = 1.037(16)$ [2] (2003) $r_Z = 1.086(12)$ [3] (2004) $r_Z = 1.047(16)$ [4] (2005) $r_Z = 1.045(4)$ [5] (2011)
μ^- -p scattering and Lamb Shift spectroscopy	$\langle r_{ch} \rangle = 0.84087(39)$ [1]	$r_Z = 1.082(37)$ [1]

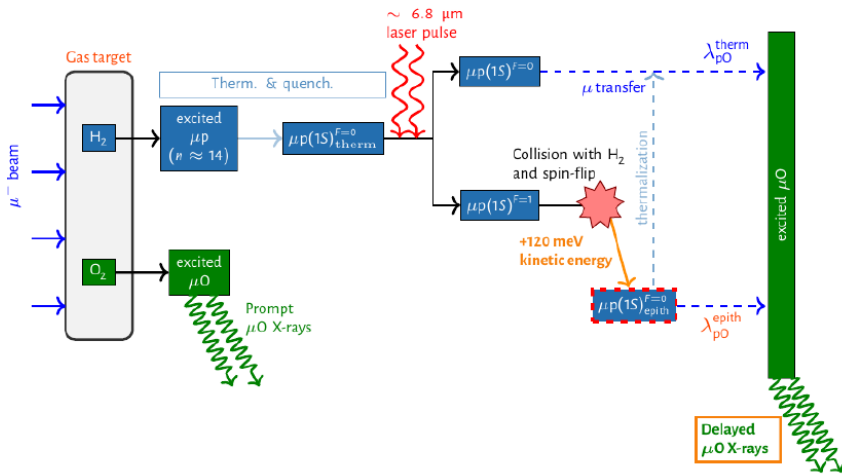


Figure 1. Schematic illustration of the principle of the FAMU experiment. After the initial phase of thermalization, a laser pulse will induce the singlet to triplet transitions in the muonic hydrogen atoms. Further collisions with H_2 molecules will convert back $F=1$ states to $F=0$ states with $\sim 0.2 \text{ keV}$ kinetic energy ($\sim \Delta E^{HFS}$). Finally, the muon is transferred from (μ^-p) to the higher Z admixture gas and the characteristic X-ray K-lines from (μZ^*) cascade are observed.

One can thus measure ΔE_{HFS} with a relative accuracy $\sim 10^{-5}$ and determine, via QED calculations, the proton Zemach radius with high precision.

The FAMU experiment will be performed in steps, starting from the study of the transfer rate from muonic hydrogen to another higher- Z gas (2014-2016) and ending with a full working setup (2018 $\rightarrow \dots$) with the pump laser and a cavity to determine the proton Zemach radius. The preliminary steps will allow determining the best mixture to be used inside the cryogenic target and optimize the operating conditions.

3 The experimental setup

The RIKEN-RAL muon facility is located at the Rutherford Appleton laboratory at Didcot (UK) and provides high intensity pulsed muon beams at four experimental ports. Its schematic layout is shown in the left panel of figure 2. The ISIS primary proton beam at 800 MeV/c , with a 50 Hz repetition rate, impinges from the left on a secondary carbon target producing a high-intensity pulsed muon beam,

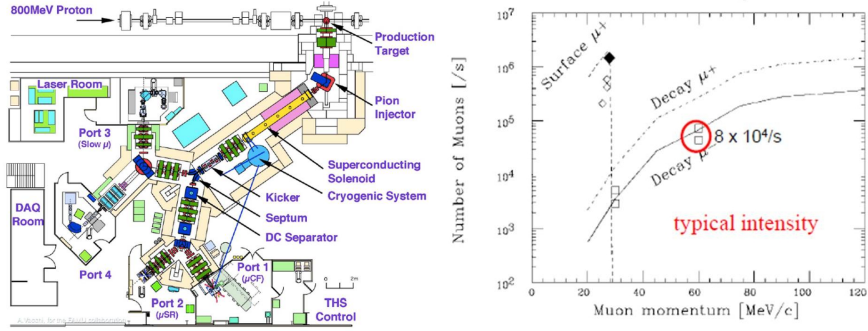


Figure 2. Left panel: layout of the RIKEN-RAL facility at RAL, with its 4 experimental ports. The FAMU experiment presently uses PORT 4 and will move to PORT 1 for the final run. Right panel: estimated intensity of the RIKEN-RAL muon beam for surface muons and decay muons in a typical square $4 \times 4 \text{ cm}^2$ area.

that reflects the primary beam structure: a double pulse structure with 70 ns pulse width (FWHM) and 320 ns peak to peak distance. The FAMU experiment makes use of the decay muon beam (muons produced outside the target from pion decay and collected by a decay solenoid) at $\sim 60 \text{ MeV/c}$. The intensity is around $8 \times 10^4 \mu^-/\text{s}$, as shown in figure 2, with an energy spread $\sim 10\%$ and an angular divergence $\sim 60 \text{ mrad}$.

3.1 The 2014 and 2015-2016 preliminary runs

The setup for the 2014 (R484) and 2015-2016 (R582) FAMU data taking are schematically shown in figures 3 and 4. A fiber-SiPMT beam hodoscope is the most upstream detector of the setup and had a

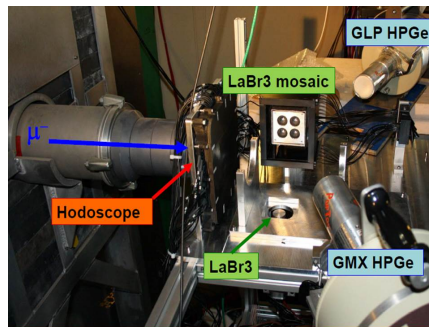


Figure 3. Preliminary setup for the 2014 FAMU run at RIKEN-RAL. From left to right, along the beamline, the 3mm pitch beam hodoscope, the target surrounded by two LaBr3 detectors and two HpGe detectors

3 mm pitch in the first 2014 run and a 1 mm pitch in the following ones. It was used to optimize beam steering inside the target. Both beam hodoscopes (with 1 mm and 3 mm pitch) have a similar structure based on BCF12 Bicron square single-clad scintillating fibers along X/Y directions (32+32 channels) read at one end by Advansid SiPMT. Difficulties encountered in developing the mechanics of the two beam hodoscopes (especially the one with 1 mm pitch) were solved via 3D printing. Details of the

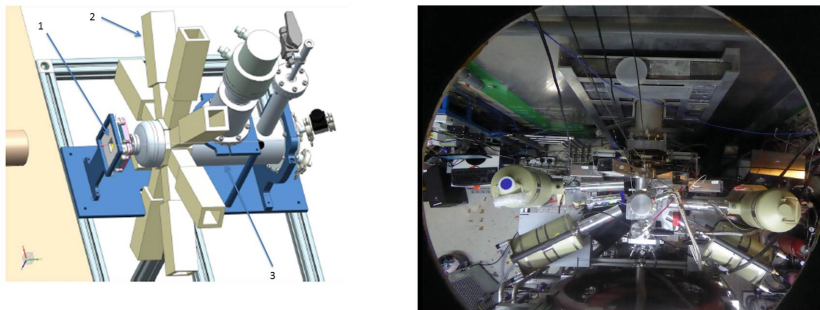


Figure 4. Left panel: layout of the FAMU experimental setup for the 2015-2016 run at RIKEN-RAL: (1) is the 1 mm pitch beam hodoscope; (2) is the crown of eight LaBr3 crystals with PMT readout, for fast X-rays detection; (3) is the cryogenic target. Right panel: view from the top of the experimental setup: the four HpGe detectors, for precise X-rays detection, are also shown.

construction and preliminary performances of the first beam hodoscope were reported in references [8] and [9].

The 1 mm pitch beam hodoscope (active area $\sim 3.2 \times 3.2 \text{ cm}^2$) was developed to be put in front of the thin Beryllium window of the cryogenic target, used in the 2015-2016 run. An effort was done to minimize materials present in the beamline. Thus Bicron BCF12 square 1 mm² scintillating fibers, with white EMA coating to avoid light cross-talk, were used. Scintillating fibers were cut at Cern with a Fiberfin4 machine, that produced ready-to-use fibers of the right length with polished ends. The main mechanics components and a picture of the detector after the beam collimator are shown in figure 5.

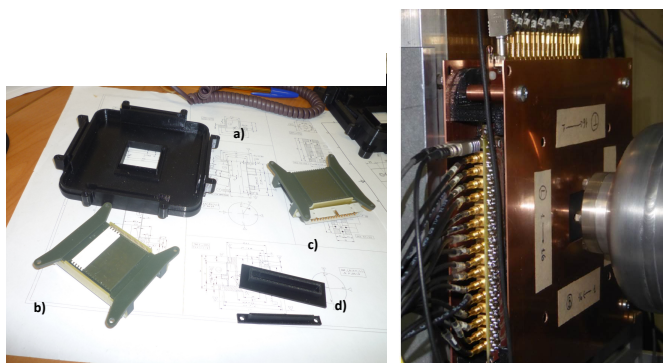


Figure 5. Left panel: main mechanical components of the 1mm pitch beam hodoscope: (a) one of the two light tight beam hodoscope cover boxes, (b),(c) X/Y plane fiber holders: in (b) some fibers are mounted, while in (c) the flat cable connector is shown, (d) cable feed-through. Right panel: picture of the beam hodoscope after the beam collimator

Scintillating fibers were read from one edge only, alternating up/down or left/right sides, by RGB $1 \times 1 \text{ mm}^2$ Advansid SiPMT with $40 \mu\text{m}$ cells. As the breakdown voltages ($\sim 29 \text{ V}$) were very similar for all SiPMTs: within 100 mV, it was possible to use a simplified front-end electronics with respect

to the one of the previous 3 mm pitch beam hodoscope, derived from the INFN TPS project ¹. All channels of the same plane (x,y) of the 1mm pitch beam hodoscope were instead powered by a single HV channel and the output signals were directly fed into a fast FADC ². Signals were routed from the PCB's, where the SiPMTs were mounted, to the external MCX cables, going to the FADC, via a short flat cable. The impedance mismatch of this cable was tested and found negligible. Figure 6 shows the FADC waveform for a typical channel, where the two pulses beam structure is evident (left panel) and the reconstructed x,y beam profiles from the integrated charge information. As expected, the beam

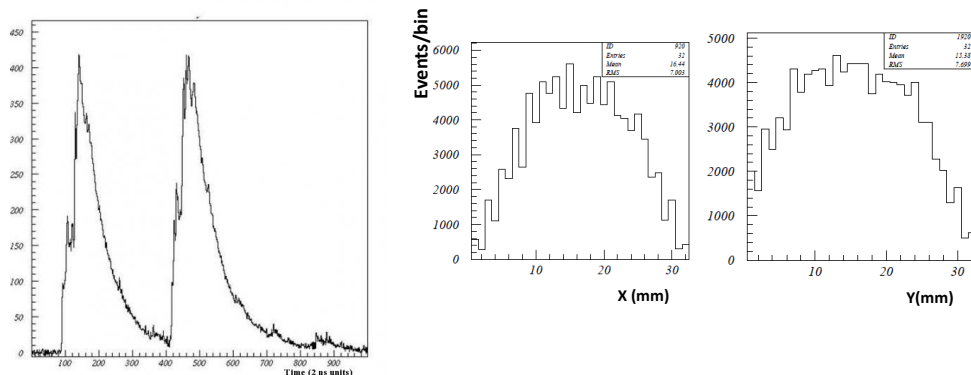


Figure 6. Left panel: waveform, as recorded by V1742 FADCs, for a typical channel of the 1 mm pitch beam hodoscope. Right panel: x/y beam profile, with standard optics, as recorded by integrating the waveform signals during the 2016 data taking.

profile is dominated by the size of the collimator and has an RMS $\sim 7 - 8$ mm.

The target, used in the 2014 run, was an Al cylindrical vessel ³ filled with a high-pressure gas. In the following runs, it was replaced by a cryogenic one. The layout of the cryogenic target is shown in the left panel of figure 7, where the percentage of stopped muons as a function of the beam momentum is shown nearby. Emitted X-rays are detected with high precision Germanium detectors (HpGe) and fast $\text{LaBr}_3\text{:Ce}$ detectors. Two HPGe detectors (one small area ORTEC GLP detector and one ORTEC GMX detector) were used in the 2014 run, while in the following runs two additional HPGe detectors from RIKEN-RAL were also used. In the 2014 run a mosaic of four 0.5-inch diameter, 0.5-inch length $\text{LaBr}_3(5\%\text{Ce})$ read by Hamamatsu R11265-200 UBA photomultipliers and a single 1-inch diameter, 1-inch length Brilliance 380 LaBr_3 crystal read by a Phillips XP2060 photomultiplier were used. In the following runs, the LaBr_3 mosaic was replaced by a crown of eight 1-inch LaBr_3 detectors read by Hamamatsu R11265-200 UBA photomultipliers, with an active divider, as shown in figure 7. The LaBr_3 detectors were read through 500 Mhz, 14-bit digitizer (CAEN V1730) with a $5\mu\text{s}$ window after the trigger, provided by the RF of the beamline, while for the HPGe detectors a slower 100 MHz, 14-bit digitizer (CAEN V1724) was used. In addition, during the 2016 data new X-rays detectors, developed for PET, based on PrLuAG and CeCAAG crystals and read out by Hamamatsu TSV SiPMT arrays, were introduced to instrument the volume under the cryogenic target [10].

¹ each TPS electronic board, with 8 individual channels, provided individual SiPMT voltage regulation, signal amplification and shaping and signal discrimination and trigger capability. Individual output signals were then fed into a CAEN V792 QADC, to measure the charge integrated signal

² CAEN V1742 FADC with 5 Gs/s, 12 bit, 1 Vpp dynamic range in VME standard

³ with a 125 mm bare diameter and a 260 mm length, it had a 2.8 liters volume. The walls had a thickness of 7 mm, except the entrance window thinned to 4 mm.

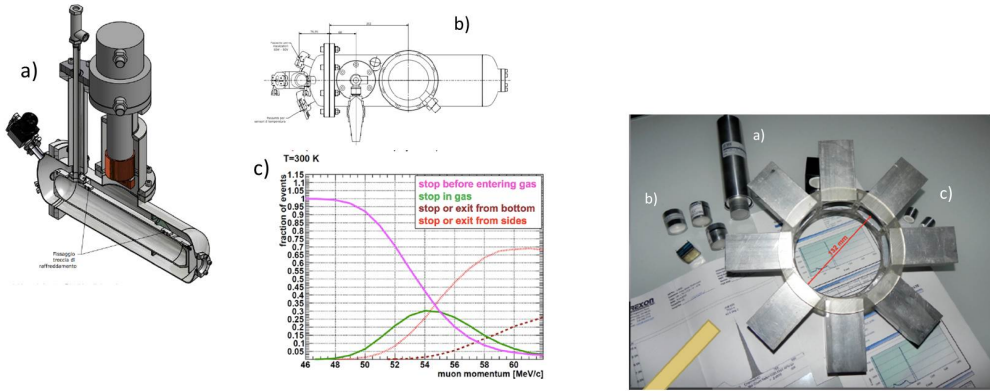


Figure 7. Right panel: (a) layout of the cryogenic target; (b) top view of the cryogenic target; (c) stopping of muons inside the target at $T=300\text{K}$. Left panel: a picture of the eight 1" LaBr3(Ce) detectors arranged in a star. (a) Hamamatsu R11265-200 UBA PMTs; (b) 1" LaBr3(Ce) crystals; (c) mechanics arrangement

3.2 The setup for the final step of the FAMU experiment.

To excite the HFS transition, a laser tunable at a wavelength around $\lambda_0 \sim \frac{2\pi\hbar c}{\Delta E_{HFS}} \sim 6.785 \mu\text{m}$ will be used. In reference [11], the main requirements on the laser system, such as energy ($\geq 0.25 \text{ mJ}$) and linewidth precision ($\lambda_0 \leq 0.07 \text{ nm}$) are discussed. The layout of the proposed laser system, under development at the Electra laboratory (Ts), is schematically shown in figure 8. A scheme based on direct difference frequency generation in nonlinear crystals, using a Q-switched Nd-Yag laser and a tunable Cr:forsterite laser will be used and is presently under test [12].

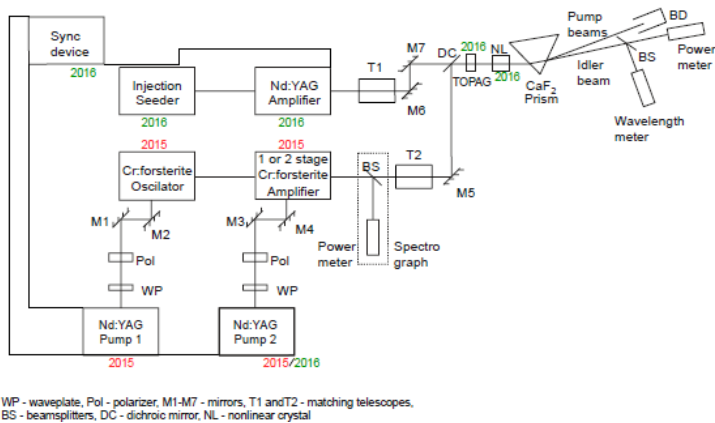


Figure 8. (Structure of the proposed mid-IR laser, under development at Electra (Ts). Wp: waveplate, Pol: polarizer; M1-M7: mirrors; T1-T2: matching telescopes; BS: beamsplitter; DC: dichroic mirror; NL: nonlinear crystal.

To increase the probability of the spin-flip ($F=0$ to $F=1$) process either the target temperature may be lowered or a multipass cavity may be used: see reference [13] for an example. With a multipass cavity that provides $\sim 2 \times 10^3$ reflections, the spin-flip probability would reach a reasonable $\sim 12\%$ value, that makes the experiment feasible. Studies of a suitable multipass cavity, that may accomodate the available cryogenic target, are under way inside the FAMU collaboration.

4 Detector performances and preliminary results

The aim of the 2014 run (R482) was to test the suitability of the proposed setup for the foreseen measurement: in particular the detection of the characteristic X-rays in a large background environment. The detection of characteristic X-rays from $LaBr_3$ detectors was cross-checked with two high precision HpGe detectors. As an example, for an $H_2 + 2\%Ar$ filled target, figure 9 shows the spectra detected by the HPGe detectors and the $LaBr_3$ crystals. All characteristic X-ray lines from the Ar

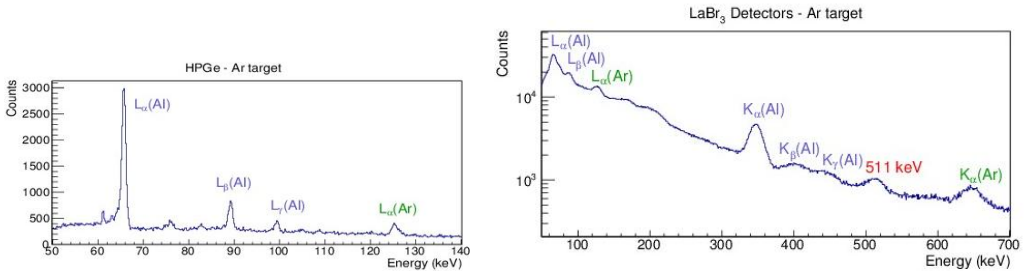


Figure 9. Left panel: characteristic X-rays lines, as detected by the HPGe detectors. Right panel: the same as detected by the $LaBr_3$ detectors.

admixture are detected, showing the correctness of the method.

Regarding the time distribution of the events, figure 10 shows an example of the time evolution of the X-ray spectrum for the $H_2 - CO_2$ target. The prompt peaks, corresponding to the two beam spills, are followed by a tail populated by the products of muon decay. From the events in the tails, the lifetime of muonic atoms may be estimated. Results are reported in table 2 and are compatible with previous ones, as reported in reference [14].

Table 2. Lifetimes of some muonic atoms in ns, as determined in the FAMU 2014 run.

	FAMU [8] (ns)	T. Suzuki <i>et al.</i> [14] and references therein (ns)
μC	2011 ± 16	2026 ± 1.5
μAl	879 ± 28	864 ± 2
μO	1824 ± 46	1795 ± 2
μAr	564 ± 14	537 ± 32
μp	2141 ± 98	2194.53 ± 0.11

Studies are under way to determine the transfer rate from hydrogen to the gas mixture contaminants (Argon or Oxygen), using the time evolution of the X-rays events inside the Argon (Oxygen) peak.

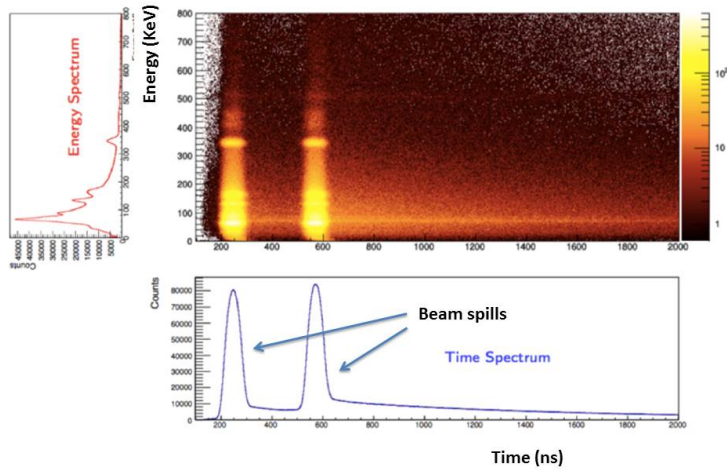


Figure 10. A snapshot of the detected X-ray spectrum (energy vs time). The two peaks are due to the two pulses structure in the incoming muon beam.

5 Conclusions

The feasibility of the method proposed by the FAMU Collaboration to determine the proton Zemach radius has been demonstrated with preliminary measurements at RIKEN-RAL: in particular the possibility to use a high-rate X-rays detection system based on $LaBr_3$ crystals.

The mid-IR pulsed laser and the multipass cavity are under development, showing that a final data taking in 2018 is feasible.

References

- [1] R.Pohl *et al.*, Nature **466** 213-216 (2010); Antognini *et al.* Science **339** 417-420 (2013).
- [2] Dupays *et al.* Physical Review **A68**, 052503 (2003).
- [3] J L Friar and I Sick, Phys. Lett. **B579** 285-289 (2004).
- [4] A.V. Volotka *et al.* Eur. Phys. J. **D33** 23-27 (2005).
- [5] Distler *et al.* Phys. Lett. **B696** 343-347 (2011).
- [6] P.J.Mohr *et al.*, Rev. Mod. Phys. **84**, 1527-1605 (2012) [CODATA].
- [7] D.Bakalov *et al.*, Phys. Lett. **A172** 277-280 (1993); A. Vacchi *et al.*, SPIE Newsroom (2012) DOI: 10.1117/2.1201207.004274.
- [8] A. Adamczak *et al.*, JINST **11/05** P05007 (2016).
- [9] R. Carbone *et al.*, JINST **10/3** C08007 (2015).
- [10] M.Bonesini *et al.*, PoS EPS-HEP2015 **244** (2015).
- [11] A. Adamczak *et al.*, Nucl. Instr. Meth. **B281** 72-76 (2012).
- [12] L.I.Stoichev *et al.*, Proc. SPIE **9135**, 91350J (2014).
- [13] J.Vogelsang *et al.*, Optics Express **22**, 13050 (2014).
- [14] T. Suzuki *et al.*, Phys. ReV. **C35** 2212-2224 (1987).